Vibration harvesting process of olive trees based on response surface methodology and rigid-flexible coupling simulation

Kehua Dang[1], Zijie Niu[1*], Haotian Mu[1], Weike Lan[1], Xu Zhang[1], Di Xin[1], Jun Zhang[1], Yongjie Cui[1,2]

(1. *College of Mechanical and Electronic Engineering, Northwest A & F University, Yangling 712100, Shaanxi, China*;
2. *Key Labouratory of Agricultural Internet of Things, Ministry of Agriculture and Rural Affairs of the People's Republic of China, Yangling 712100, Shaanxi, China*)

Abstract: A trunk-vibrating screen is widely used in olive harvesting machinery. Because of the irregularity of fruit recovery efficiency, the recovery efficiency fluctuates greatly. Vibration harvesting parameters are important factors affecting the percentage of olive harvest. Therefore, the study of vibration picking parameters is of great significance for olive harvest. Vibration parameters, governed by tree morphological parameters, strongly influence the efficiency of vibration harvesting. In this study, a combination of response surface simulation and harvesting experiments was used to investigate the relationship between morphological and vibration harvesting parameters in "three open-center shape" olive trees. First, force analysis and experimental measurements were performed on the olive fruit, and the Box-Behnken design was used to obtain the vibration parameters through finite element simulation and to establish the response surface model of the parameters (main trunk diameter, main trunk height, main branch angles *A* and *B*) and the vibration parameters (vibration frequency and vibration force) of the "three open-center-shape" olive trees. In addition, the mapping relationship between tree shape parameters and vibration parameters was obtained. The results show that the 90% quantile of the acceleration of abscission of olives is 1113.35 m/s^2; the average correlation coefficient between the simulation and the experiment results was 0.73, and the simulation was a good representation of the experimental results. When the tree shape was "three open-center", the trunk diameter and height were related to the vibration harvesting parameters; the average harvesting efficiency of olives was 91.22%, and the resonance frequency of the monitoring points was similar to that of the simulation results. This study provides a reference for the design of vibration harvesting equipment and fruit tree shaping.

Keywords: olive, three open-center shape, vibration harvesting, modal analysis, rigid-flexible coupling simulation, acceleration response

DOI: 10.25165/j.ijabe.20251803.8792

Citation: Dang K H, Niu Z J, Mu H T, Lan W K, Zhang X, Xin D, et al. Vibration harvesting process of olive trees based on response surface methodology and rigid-flexible coupling simulation. Int J Agric & Biol Eng, 2025; 18(3): 25–36.

1 Introduction

Olive tree fruits are an economic crop from the Oleaceae tree family, which is one of the four major edible oil tree species worldwide. Furthermore, olive oil has extremely high economic value and is extensively used in chemicals, cosmetics, textiles, and many other products[1,2]. This crop is widely distributed in countries bordering the Mediterranean, with a harvested area of more than 12 million hectares[3]; however, harvesting represents a large proportion of the olive oil production cycle. In some situations, the expense of olive harvesting can be more than 50% of the production revenue[4].

During the traditional harvesting process, seasonal workers stand on the ground to pick low-level apples and take advantage of ladders to get access to high-level fruits[5]. Workers are also vulnerable to musculoskeletal disorders due to carrying heavy loads and repetitive hand and upper body actions, and the hazards of falling from ladder climbing and descending[6]. The gradual increase of labor cost and shrinking labor pool have added severe burdens on the harvesting process[7,8]. In recent decades, the mechanized harvesting of olives has attracted extensive attention for reducing costs and improving harvest efficiency. More research on the relevant theory and technological advancements of harvesting robots is necessary to achieve harvesting mechanization and operation automation, lower operator labor intensity, free up more farm labor force, compress agricultural production costs, satisfy timely harvesting demands, increase harvest productivity, alleviate occupational injuries, and minimize financial losses. Robotics has become increasingly crucial in contemporary agriculture and has become an integral part of precision agriculture. Robotic harvesting-related technical research advances agriculture science and technology to accelerate agricultural modernization[9-11].

It is imperative that competent technologies be developed and improved through research and field applications[12]. A trunk-vibrating screen is the most widely used harvesting machine[13]. Zhang et al.[14] summarized the development of shaking harvesting machines for fresh fruits, and Mhamed et al.[15] also systematically summarized the development of apple harvesting machines. Yu et

Received date: 2024-01-08 **Accepted date:** 2025-01-02

Biographies: Kehua Dang, ME, research interest: intelligent agricultural machinery equipment, Email: dangkh@nwafu.edu.cn; **Haotian Mu**, ME, research interest: intelligent agricultural machinery equipment, Email: 635406182@nwafu.edu.cn; **Weike Lan**, ME, research interest: target recognition and localization algorithm, Email: 18260873426@139.com; **Xu Zhang**, ME, research interest: intelligent agricultural machinery equipment, Email: zx0825@nwafu.edu.cn; **Di Xin**, ME, research interest: piezoelectric actuator, Email: cindy0536@nwafu.edu.cn; **Jun Zhang**, PhD, Lecturer, research interest: ultrasonic motor drive and control technology, Email: junzhang@nwafu.edu.cn; **Yongjie Cui**, PhD, Professor, research interest: modern intelligent agricultural equipment and technology, Email: cuiyongjie@nwsuaf.edu.cn.

***Corresponding author: Zijie Niu**, PhD, Associate Professor, research interest: intelligent agricultural machinery equipment. College of Mechanical and Electronic Engineering, Northwest A&F University, 22 Xinong Road, Yangling 712100, Shaanxi, China. Tel: +86-15191862878, Email: niuzijie@nwafu.edu.cn.

al.[16] summarized Apple's on-site grading and sorting technology equipment. Compared with manual harvesting, mechanized harvesting can greatly improve harvest efficiency, but the fruit collection rate is irregular, ranging from 50% to 90%, and the fruit is easily damaged when the harvest percentage is extremely high[17-20]. Factors that influence the percentage of olives harvested include vibration harvesting parameters and the tree structure[21-24]. Therefore, the study of vibration harvesting parameters is of great significance for the harvesting of olive fruits.

Many researchers have studied the vibration harvesting parameters to achieve efficient mechanized harvesting[25-27]. Leone et al.[28] used an orbital trunk shaker to determine the optimal vibration frequency and duration for various olive tree varieties. Fu et al.[29] established a finite element model of sea buckthorn using measurements and determined suitable harvesting parameters. Chen et al.[30] designed a harvester with orthogonal eccentric blocks and experimentally demonstrated that when the rotational speed of the vibration mechanism was 7.83 r/s and the vibration time was 10 s, the maximum harvest rate was 76.5%. Yang et al.[31] developed a rigid-flexible coupling simulation of a fruit tree and a harvester for a shaped pistachio tree and optimized the vibration parameters through the response surface to obtain an optimum vibration frequency of 18 Hz and a harvesting percentage of 90% for a vibration force of 3000 N. Du et al.[32] used orthogonal tests to optimize the vibration harvesting parameters for oil tea, showing that the fruit harvesting rate was 72.3% at 6 r/s and 80 mm amplitude. Chen et al.[33] conducted a response surface test on a standardized hedgerow cultivation model of Lycium barbarum plants and obtained the best combination of harvesting parameters: a vibration frequency of 38.73 Hz, a brush speed of 14.21 mm/s, and an insertion depth of 26.07 mm, under which the harvest rate of ripe fruit was 83.65%.

Researchers have focused on the effect of fruit-tree parameters on vibration harvesting. For example, Tombesi et al.[34] conducted an experimental analysis of the effect of unproductive branches inside the olive oil canopy on vibration transmission and harvesting and showed that unproductive branches impede vibration transmission and need to be pruned. Castillo-Ruiz et al.[22] compared the effect of different pruning methods on a canopy-vibration harvester. These studies have focused more on the pruning of traditional fruit trees for better suitability for vibration harvesting[35,36]; however, there are currently few studies on the effect of morphological parameters of shaped fruit trees on vibration parameters.

The aim of this study is to assess the influence of morphological parameters on vibration frequency and vibration forces in "three open-center" shaped olive trees. The specific objective is to achieve a harvest percentage of more than 90% for "three open-center" shaped olive trees. The effect of the morphological parameters of the olive tree on the vibration frequency and force was investigated using response surface methodology and simulations, and the simulation model was validated experimentally.

2 Materials and methods

2.1 Overall process description

In this study, the force of the olive fruit was analyzed by the principle of the harvester, the conditions of the fruit falling off were analyzed, the corresponding vibration test was carried out at the experimental site, and the corresponding data were measured. Then the finite element model of olive tree was established, and the response surface experiment was designed. The rigid-flexible coupling structure model was established, and the modal analysis was carried out. Finally, simulation data and experimental data were analyzed and compared to verify the feasibility of this research method. The specific flow chart is shown in Figure 1.

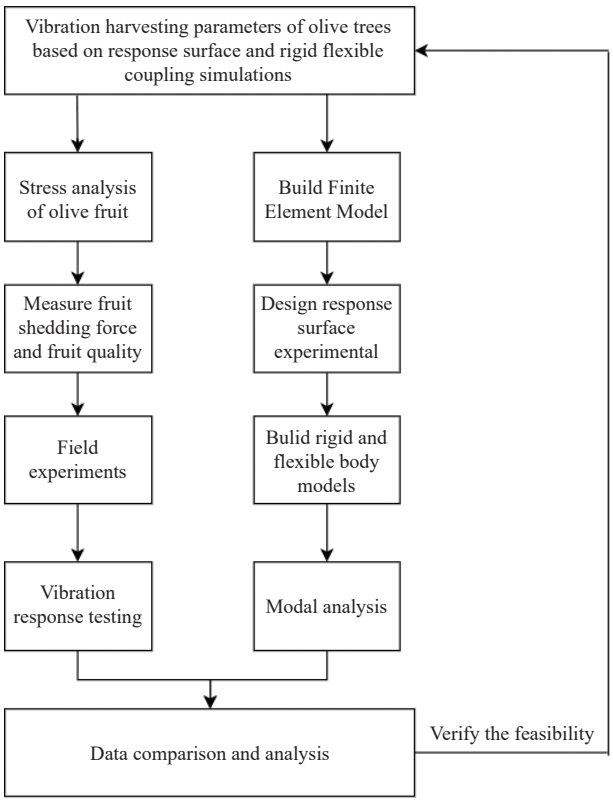

Figure 1 Experiment general flow chart

2.2 Working principle of the harvester

Trunk shakers are the most used vibratory fruit harvesters and consist of a single eccentric mass rotating around an axis[37]. Xu et al.[38] demonstrated that a single eccentric block vibration produced the largest vibration acceleration when operated on fruit trees; therefore, a single eccentric block vibration was selected for this study. The harvesting principle is as follows: The eccentric mass is fixed to the fruit tree and rotates at a high speed to generate a centrifugal force, which is then transferred to the fruit tree, which receives forced vibration and transfers the vibration energy to the fruit, thus causing the fruit to generate an inertial force. When the inertial force is greater than the restraining force between the fruit and the stem, the fruit falls, and the harvesting is completed[39]. The principal diagram of the orbital vibration harvester is shown in Figure 2. In the model shown in Figure 2, the high-speed rotation of the eccentric block produces a centrifugal force, forming a circular excitation, which can be decomposed into components of equal size with a 90° phase difference located in the x- and y-axis directions, as shown in Equation (1).

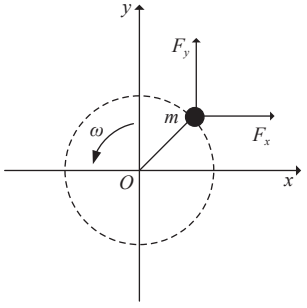

Figure 2 Principal diagram of trunk shakers

$$\begin{cases} F_x = m_e\omega^2\cos(\omega t) \\ F_y = m_e\omega^2\sin(\omega t) \end{cases} \quad (1)$$

where, F_x and F_y are the component forces of the centrifugal force in the x- and y-axis directions, respectively, N; m_e is the eccentric mass, kg; e is the eccentricity, m; ω is the angular velocity of rotation, rad/s; and t is the time of rotation, s.

The experimental site selected for this study was in a commercial orchard in the town of Lishui, Longnan, Gansu Province, China (coordinates: 33°26′49″N, 104°46′350″E, altitude: 1243 m), where the main variety of olive trees grown in the orchard was Leccino, and all were oil olive. To ensure a high yield of individual olive trees, the orchards are manually shaped and pruned every year. More than 90% of the olive trees are "three open-center shape" trees, which are shaped such that the middle of the crown remains open, with three main branches evenly distributed at an angle of approximately 45° to the main stem, each of which is conical in shape. Figure 3 shows the orchard of two olive trees pruned in summer and winter, and the olive trees shown are typical "three open-center shape" trees.

a. In summer b. After winter pruning

Figure 3 Three open-center shape olive trees

2.3 Analysis of fruit abscission conditions

When the vibration energy applied by the harvesting machine is transmitted along the branch to the fruit, the fruit undergoes accelerated motion and is subjected to inertial forces. When the inertial force is greater than the restraining force between the fruit and stem, the fruit is abscised. According to Castro-Garcia et al.[23], fruit acceleration can be used as a criterion for fruit abscission. Therefore, in this study, acceleration was used to discriminate fruit abscission. Force analysis of olive fruit was performed as shown in Figure 4, where F_c is the restraining force between the fruit and stem (N), a is the acceleration of the fruit, a_n, a_τ are the normal and tangential components of the acceleration of the fruit (m/s²), F_a is the inertial force generated by the vibration of the fruit, F_n, F_t are the normal and tangential components of the inertial force (N), G is gravitational force (N), G_n, G_t are the normal and tangential components of gravitational force (N), m is the mass of the olive fruit (kg), and φ is the angle (°) between the stem and the direction of gravity when the fruit is abscised.

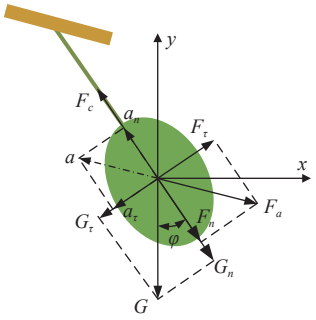

Figure 4 Fruit force analysis diagram

When F_t is greater than the tangential component of the gravitational force G_t, the sum of the normal components of the gravitational forces G_n and F_n is greater than the restraining force F_c between the fruit and stem, and the fruit is abscised, as shown in Equation (2).

$$\begin{cases} F_t \geq G\sin\varphi \\ F_n \geq F_c - G\cos\varphi \end{cases} \quad (2)$$

The effect of gravity was neglected because the gravity force of the fruit is minimal compared to that of other forces during vibration[40,41]. Both the tangential and normal components of the inertial force can be expressed using acceleration, as shown in Equation (3).

$$\begin{cases} F_t = ma_t \\ F_n = ma_n \end{cases} \quad (3)$$

Substituting Equation (3) into Equation (2) yields Equation (4):

$$\begin{cases} ma_t \geq 0 \\ ma_n \geq F_c \end{cases} \quad (4)$$

The conditions for olive fruit abscission are shown in Equation (5).

$$a = \sqrt{a_n^2 + a_t^2} \geq \frac{F_c}{m} \quad (5)$$

Thus, the abscission acceleration of the olive fruit can be simplified as the ratio of the restraining force between the fruit and stem to the fruit mass. During the ripening period, the abscission force of the fruit was measured using a tension meter (SK-50, Shanghai Siwei Instrument Manufacturing Co., Ltd., Shanghai, China), which measures the peak force by applying a continuously increasing force in the opposite direction of the branch until the fruit abscises and records the peak force as the fruit stem restraining force[42]. The experimental test scene is shown in Figure 5. The fruits' mass was measured using an electronic scale with an accuracy of 0.01 g.

Figure 5 Measurement of fruit stem restraining force

2.4 Simulation of vibration harvesting parameters

2.4.1 Finite element model of the olive tree

Assuming that the main branches of the olive tree are in a plane perpendicular to the ground, all three main branches are identical, and the branches have a circular cross-section, a three-dimensional model of the olive tree was generated using SolidWorks. Three thin branches were created on each main branch to represent the fruit stalk (nodes a-c). The constructed olive tree model is shown in

Figure 6, as are the three branches constructed.

The three-dimensional model was imported into ANSYS 19.0 for simulation analysis. Based on Niu et al.[43], the density of the olive tree was set to 1024 kg/m³. The stiffness matrix C is shown in Equation (6), and the damping ratio of 0.04 in SOLID185 was selected. SmartSize was used for meshing, and displacement constraints were applied to the bottom surface of the olive tree to simulate the root fixation effect[44].

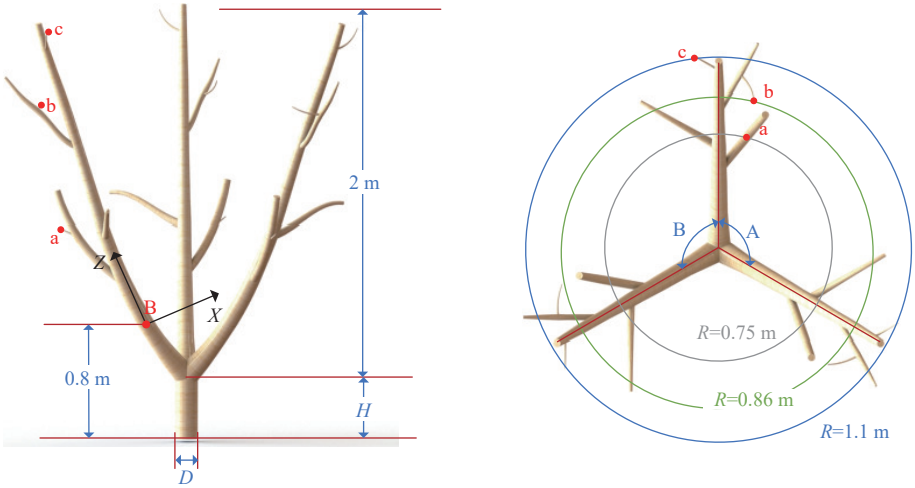

Figure 6 Three-dimensional model of olive tree

$$C = \begin{bmatrix} 4.35 & 3.03 & 2.59 & 0 & 0 & 0 \\ 3.03 & 4.51 & 2.08 & 0 & 0 & 0 \\ 2.59 & 2.08 & 10.8 & 0 & 0 & 0 \\ 0 & 0 & 0 & 1.05 & 0 & 0 \\ 0 & 0 & 0 & 0 & 1.12 & 0 \\ 0 & 0 & 0 & 0 & 0 & 0.95 \end{bmatrix} Gpa \quad (6)$$

2.4.2 Response surface experimental design

Based on actual measurements and observations, it was determined that the morphological parameters of various olive trees differed mainly in trunk diameter, height, and angle between branches. Trunk diameter is related to the age of the tree; in general, the older the tree, the larger the trunk diameter, whereas the trunk height and angle between branches are determined during the shaping process. Thirty olive trees aged between 7-15 a were randomly selected from the olive orchards and their trunk diameter D, height H, and angles A and B between the main branches were measured. Figure 7 shows the measured results of olive tree morphological parameters in the form of quartile plots.

The trunk diameter (D), trunk height (H), and main branch angles (A and B) were selected as test factors, where the ratio of the diameter of each branch section to the trunk diameter was constant. The vibration harvesting frequency and excitation force were selected as the responses. The upper and lower limits of the test factors were selected based on the actual measurements, and simulations were performed to obtain the response values. A four-factor, three-level Box-Behnken response surface test with three focal points and 27 sets of trials was designed using Design Expert 12.0.3 software. The test factor coding table is listed in Table 1.

Response surface methodology (RSM) is a common tool for analyzing the influence of factors on the responses and is widely used in agricultural research[45,46]. The response variable can be fitted to the general form of a quadratic polynomial model as shown in Equation (7).

$$Y = \beta_0 + \sum_{i=1}^{4} \beta_{ii} X_i^2 + \sum_{i=1}^{3} \sum_{j=i+1}^{4} \beta_{ij} X_i X_j \quad (7)$$

where, Y is the response variable, X_i is the component i of the influence factor, and β_0,β_i,β_{ii}, and β_{ij} are terms of regression coefficients for intercept, linearity, square, and interaction, respectively.

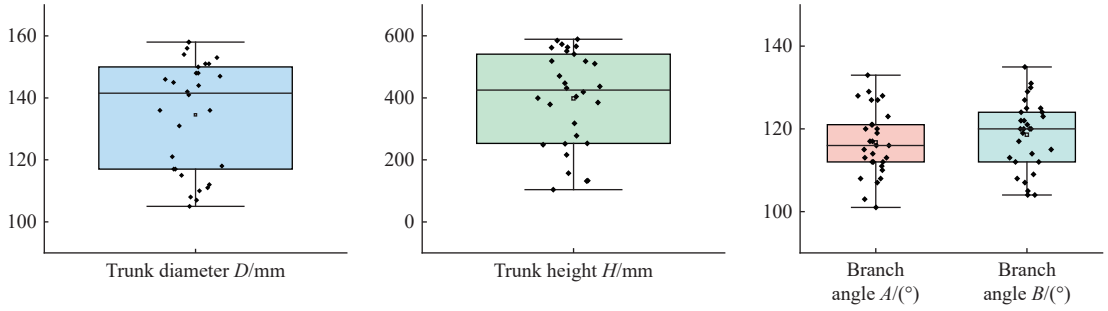

a. Trunk diameter b. Trunk height c. Branch angles

Figure 7 Statistics of olive tree morphological parameters

Table 1 Experimental design and level of Box-Behnken design

Factors	–1	0	1
Trunk diameter D/mm	100	130	160
Trunk height H/mm	500	600	700
Branch angle A/(°)	100	125	150
Branch angle B/(°)	100	125	150

2.4.3 Experiment and rigid-flexible coupling simulation

To verify the reliability of the simulation results, an olive tree was randomly selected from the test garden for the experiment, as shown in Figure 8. The selected olive tree had a trunk diameter D of 153 mm, a trunk height H of 510 mm, and main branch pinch angles A and B of 125° and 130°, respectively.

1. Vibrating motor 2. Acceleration meter 3. Computer 4. Data collector

Figure 8 Acceleration measurement experiment

To avoid the effects of fruit and leaf abscission, a small vibrating motor with an adjustable speed was used to provide the vibration force, and only a small proportion of the leaves and fruit were shed during the experiment. There were two identical eccentric blocks in the vibration motor. The mass of each eccentric block was 0.415 kg, the eccentric distance was 18.4 mm, and the vibration frequencies used were 10, 15, 20, 25, and 30 Hz. The excitation position was selected to be 800 mm above the ground, as shown in Figure 6, and the vibration motor was fixed using U-bolts. An accelerometer (DH311E, Donghua Testing Technology Co., Ltd., Taizhou, China) and data collector (DH5922, Donghua Testing Technology Co., Ltd., Taizhou, China) were used to measure the acceleration of the olive tree at the acceleration points on the main branch, as shown in Figure 8, and a measurement point was selected every 350 mm on the main branch, as shown in Figure 9.

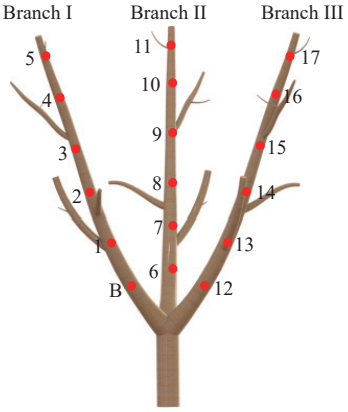

Figure 9 Measuring points distribution

A model of the olive tree and vibration motor was established using SolidWorks and imported into ADAMS. The vibration motor was set as a rigid body, and a modal neutral file (mnf) of the olive tree was calculated using the ANSYS software. Subsequently, the generated mnf file was imported into ADAMS to replace the rigid body and generate a flexible body model of the olive tree. The rigid–flexible model composed of the olive tree and vibration motor was a coupled model, as shown in Figure 10. Different vibration frequencies were obtained by varying the speed of the eccentric block and varying its mass to achieve different vibration forces.

After obtaining the acceleration values in the three directions at the selected points through simulations and experiments, an analysis was performed using the synthetic acceleration values, that is, the root mean square values of each acceleration in the *x*-, *y*-, and *z*-directions (a_x, a_y, and a_z), as shown in Equation (8)[23,47].

$$a_{3D} = \sqrt{a_x^2 + a_y^2 + a_z^2} \tag{8}$$

2.4.4 Method of acquiring response

Modal analysis can be used to determine the intrinsic properties of the olive tree, and therefore determine the range of vibrational harvesting frequencies. The Block Lanczos method was used for modal analysis in this study[48]. Generalized eigenvalues were solved using a sparse matrix, that is, the Lanczos recursion was implemented with a set of vectors. With this method, the calculations are faster and more accurate[49]. Structural vibration can be expressed as a linear combination of all-order intrinsic vibration modes, and the influence of lower-order vibration modes is greater than that of higher-order modes[29]. Therefore, lower-order vibration modes determine the dynamic characteristics of the structure. The first 20 orders of the intrinsic frequencies of the olive tree were selected for modal analysis in this study.

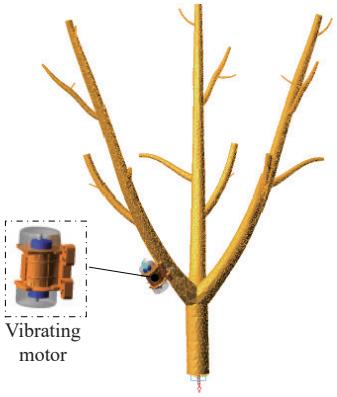

Figure 10 Rigid-flexible coupling model of olive tree-vibrating motor

After obtaining the harvesting frequency range, a sinusoidal sweep excitation with an amplitude of 100 N was applied in the *x*-direction of the excitation position (Figure 6, point B) in ADAMS, and the average synthetic acceleration of the three fruit stalk points (Figure 6, points a, b, and c) in the olive tree model was measured to obtain the optimal vibration-harvesting frequency by sweep analysis.

After obtaining the vibration-harvesting frequency, this frequency was used as the vibration motor speed, and the synthetic acceleration of the three shank points under different excitation forces was obtained by changing the mass of the eccentric block. The vibration force when the acceleration was greater than the abscission acceleration was used.

2.5 Field experiments

2.5.1 Harvesting prototype

The olive-harvesting prototype consists of a crawler chassis, housing frame, lifting mechanism, clamping mechanism, and vibration mechanism, as shown in Figure 11. Typical four-wheel or tricycle platforms can travel on flat firm terrain but are not well-suited for rough or muddy fields. Tracked platforms work better on uneven or muddy terrains[12]. The clamping mechanism uses cylinders to provide a clamping force, and the circular clamping plate rotates around the cylinders to clamp the inclined branch. The vibration mechanism consists of a motor and a semi-circular eccentric block, with two eccentric blocks on each side of the motor. The eccentric distance between the blocks can be changed by varying the angle θ between the two eccentric blocks to adjust the vibration force, as expressed in Equation (9). The total mass of the four eccentric blocks is approximately 24.76 kg, and the eccentricity distance is 47.5 mm when $\theta = 180°$.

$$F = me\omega^2 \sin\frac{\theta}{2} \tag{9}$$

where, F is the vibration force, N; m is the mass of the eccentric block, kg; e is the eccentricity at $\theta = 180°$; ω is the angular velocity of rotation, rad/s; and θ is the angle between the eccentric blocks, (°).

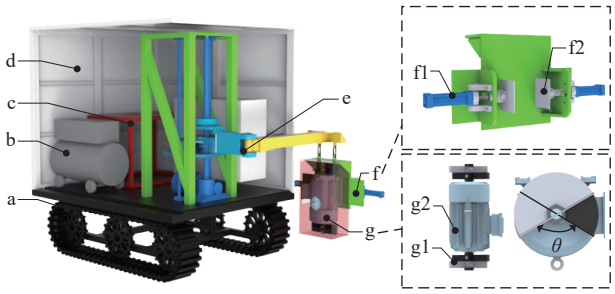

1. Track chassis 2. Air compressors 3. Generators 4. Shell frame 5. Lifting mechanism 6. Clamping mechanism 6a. Cylinder 6b. Arc splint 7. Vibration mechanism 7a. Eccentric block 7b. Motor

Figure 11 Schematic of olive harvesting prototype

2.5.2 Harvest percentage

Three olive trees with a clamping height of 800 mm were selected for a harvesting trial during the maturity period of the olive tree. The harvest percentage was calculated using the weight, as shown in Equation (10):

$$R_h = \frac{m_v}{m_v + m_s} \times 100\% \quad (10)$$

where, R_h is the percentage of harvest, %; m_v is the weight of the olive fruit harvested by vibration, kg; and m_s is the mass of the remaining manually harvested olives, kg.

2.5.3 Vibration response testing

To verify the results of the response surface, a post-harvest olive tree, with trunk diameter D of 153 mm, trunk height H of 118 mm, main branch angle A of 130°, and main branch angle B of 135° was selected for dynamic response testing. The dynamic response of the olive trees was measured using an acceleration measurement system. The acceleration measurement system consisted of a harvesting prototype, four three-axis acceleration sensors (WT901, Shenzhen Wit-motion Co., Ltd.), and data recording software, as shown in Figure 12.

Four detection nodes were selected on the olive tree, where node 1 was located on the main branch, and the other three nodes were located on the tertiary side branches. An eccentric block angle θ = 0° was used in the experiment. When the vibration frequency was less than 5 Hz, the vibration force generated by the harvesting prototype was small. Therefore, the vibration frequency selected for the experiment was 5-25 Hz applied in increments of 2.5 Hz. A total of nine experiments were conducted.

Both the vibration frequency and vibration force are key factors affecting the acceleration response. To minimize the effect of vibration force, the average synthetic acceleration due to unit vibration force (P_{3D}, m/s²·N) is defined as shown in Equation (11).

$$P_{3D} = \frac{\bar{a}_{3D}}{F_f} = \frac{\bar{a}_{3D}}{me\omega^2} = \frac{\bar{a}_{3D}}{4m\pi^2 f^2 e} \quad (11)$$

where, $\bar{a}_{3D}$ denotes the average synthetic acceleration, m/s²; f is the vibration frequency, Hz; F_f is the vibration force corresponding to the vibration frequency f, N; m is the mass of the eccentric block, kg; and e is the eccentric distance of the eccentric block, m.

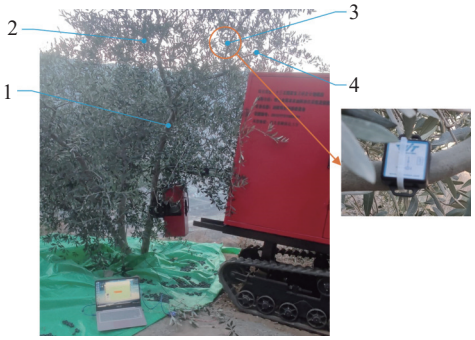

Figure 12 Acceleration measurement and monitoring positions

3 Results and discussion

3.1 Analysis of fruit abscission conditions

In the olive orchard, 100 fruits from 10 trees were selected to measure the restraining force and mass, and the Shapiro-Wilk test was used to test the fruit abscission force and fruit weight. The results showed that the p-value for both sets of data was greater than 0.05; therefore, both sets of data were normally distributed. The data were examined using box plots, and the results showed no outliers (Figure 13). The fruit weight of olives at maturity was 4.15±0.11 g, and the 95% confidence interval was 3.94-4.38 g. The mean restraining force between the fruit and stem was 3.28±0.13 N, and the 95% confidence interval was 3.00-3.56 N. The acceleration of fruit abscission was 802.29±33.09 m/s², with a 95% confidence interval of 735.80-868.79 m/s². The 90% quantile of abscission acceleration (1113.35 m/s²) was used as a measure of olive fruit abscission to ensure that the percentage of the harvest was greater than 90%.

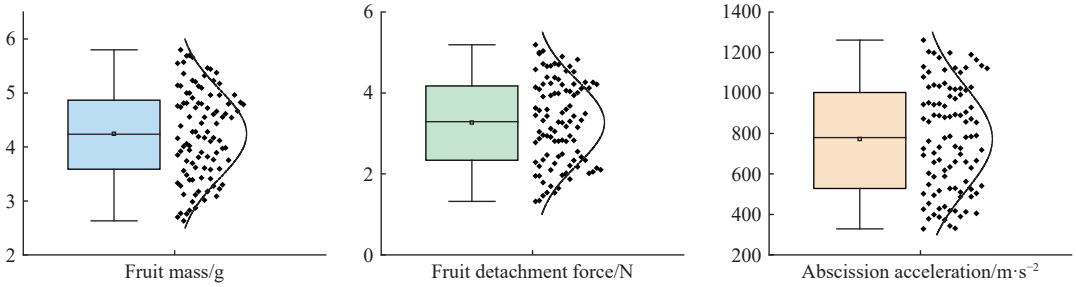

a. Fruit mass b. Fruit restraining force c. Abscission acceleration

Figure 13 Statistics of fruit mass and fruit restraining force

3.2 Experiment and rigid-flexible coupling simulation

The average synthetic acceleration values at different frequencies were obtained through vibration experiments and rigid-flexible coupling simulations, as shown in Figure 14, where "Sim" is the simulation result and "Exp" is the experimental result. At all frequencies, the synthetic acceleration on main branch I was greater than those on main branches II and III, and the point at the top of each main branch was the maximum value for that branch. Most points in the graph show similar trends; however, some points show different trends. The number of points with different trends increased significantly at a frequency of 30 Hz. This may be because the vibration motor and trunk were not fully connected during the experiment, resulting in an incomplete transmission of vibrations to the trunk at high frequencies and energy loss between

the acceleration sensor and the branch. To remove points with large errors, the acceleration differences were examined using box plots, as shown in Figure 15, and the results showed that point 5 at 25 Hz was an outlier; therefore, this group of data was removed from the subsequent analysis.

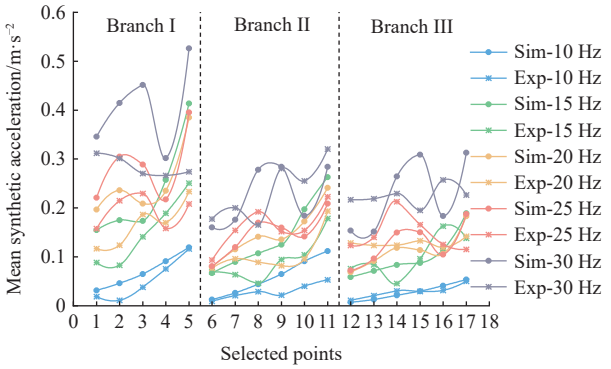

Figure 14 Comparison between rigid-flexible coupling simulation and experimental results

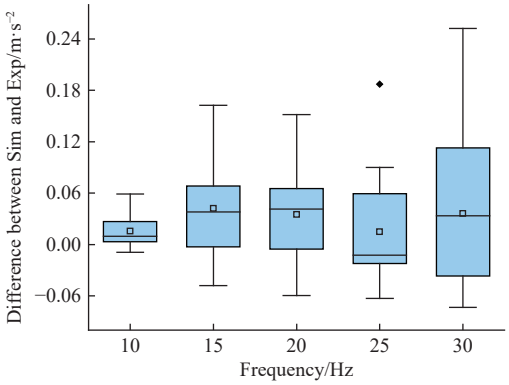

Figure 15 Box diagram of differences between simulation and experiment

The Pearson correlation coefficients between the simulation and experiment at different frequencies were calculated using the SPSS software, as listed in Table 2. The correlation coefficients at all frequencies are greater than 0.5, reaching a maximum at 15 Hz with 0.87 and a minimum at 30 Hz with 0.5. The mean correlation coefficient between simulation and experiment was 0.73, greater than that of Savary et al.[50] on citrus trees with a correlation coefficient result of 0.58, and Peng et al.[44] on jujube trees with a correlation coefficient result of 0.62. The mean relative error between simulation and experiment was 26.5%, and the mean relative error of the mean was 18.5%, which was less than that of Carvalho et al.[51] and Villibor et al.[52] on coffee trees, with mean errors of 37% and 35.9%, respectively. This indicated a strong correlation between the simulation and experiment, demonstrating that the simulation can better represent the actual vibration.

3.3 Process of acquiring response

The modal frequencies can be divided into three classes based on the results of the modal analysis, as shown in Figure 16. The first class is low frequency, and the vibrations are concentrated in the upper part of the three main branches, as shown in Figure 16a. The second class is medium-frequency, and the vibration occurs in the entire olive tree and the amplitude is relatively high, as shown in Figure 16b. The third class is high frequency, where the vibration occurs mainly in some small branches, and the amplitude is relatively small, as shown in Figure 16c. Therefore, medium-frequency vibration is suitable for vibrational harvesting of olive trees, which concurs with the results of Bentaher et al.[4] and Niu et al.[43]

Table 2 Average synthetic acceleration statistics for experiments and simulations at different frequencies

Frequency/ Hz	Mean/m·s⁻²		Standard deviation/ m·s⁻²		Pearson correlation coefficient
	Simulation	Experiment	Simulation	Experiment	
10	0.511	0.356	0.035	0.027	0.81**
15	0.155	0.112	0.092	0.056	0.87**
20	0.166	0.131	0.080	0.043	0.77**
25	0.167	0.166	0.068	0.041	0.71**
30	0.281	0.245	0.109	0.046	0.50*

Note: * indicates significant correlation at the 0.05 level; ** indicates significant correlation at the 0.01 level.

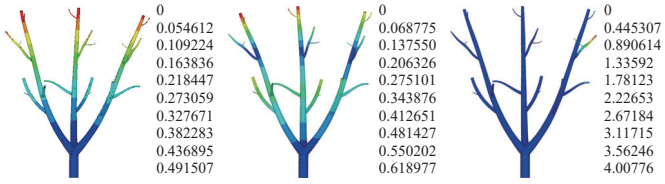

a. Low frequency (1st order) b. Medium frequency (7th order) c. High frequency (13th order)

Figure 16 Three classifications of modal analysis

According to the method described in Section 2.4.4, the acceleration versus frequency curves for the three stalk nodes (Figure 6, nodes a-c) obtained by sweep analysis in ADAMS are shown in Figure 17, in which multiple distinct resonant frequencies appear in the plot. Based on the results of the modal analysis, the appropriate vibration frequency range for test 1 was determined to be 16.87-23.04 Hz. The frequency corresponding to the point of maximum acceleration in this range was 17.43 Hz, which was considered as the vibration frequency.

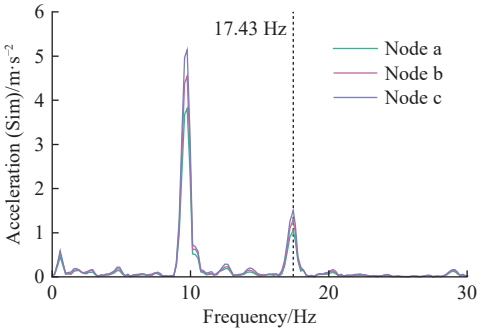

Figure 17 Acceleration-frequency curves for swept-frequency analysis

Using the obtained vibration frequencies, different vibration forces were applied by varying the mass of the eccentric block to obtain the average synthetic acceleration at the three shank points for the different vibration forces, as listed in Table 3.

Table 3 Average synthetic acceleration at fruit stalk nodes obtained by simulation

Vibration force/N		2500	5000	7500	10 000	12 500	15 000
Acceleration/ m·s⁻²	Node a	475.34	855.33	1148.88	1370.24	1522.94	1655.96
	Node b	402.68	721.68	970.65	1166.21	1304.78	1439.07
	Node c	265.05	523.86	781.1	945.94	1015.62	1218.52

The acceleration at point *c* was the least of the three sets of values; therefore, when the acceleration at point *c* reached the acceleration of fruit abscission, the accelerations at the remaining

points were greater than that of fruit abscission. With the excitation force as the variable and the acceleration at point *c* as the dependent variable, and employing SPSS for curve estimation, the fitted comparisons are listed in Table 4, with cubic fits being the best, as shown in Figure 18. When the synthetic acceleration at point *c* was the fruit-shedding acceleration, the excitation force was approximately 13 558 N, which was used as the excitation force.

Table 4 Excitation force-acceleration fitting results at point *c*

Model fit statistics			Parameter values			
Equation	R^2	*F* value	Constant	*b*1	*b*2	*b*3
Linear	0.969	124.745	150.935	0.073		
Logarithmic	0.981	206.287	–3847.586	520.063		
Inverse	0.874	27.680	1215.489	–2 594 738.190		
Quadratic	0.990	145.372	–20.697	0.125	–2.942E-06	
Cubic	0.994	107.803	–176.020	0.203	–1.330E-05	3.945E-10

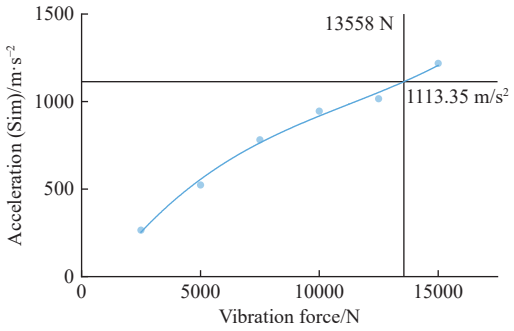

Figure 18 Excitation force results of three fits of acceleration at point *c*

3.4 Analysis of simulation experiment results

Using the four morphological parameters of the olive tree as test factors, this study obtained the response variables using the method described in Section 3.3. The experimental scheme and results are listed in Table 5. The best model was selected according to the test results, and a quadratic model was established for the vibration frequency and force; the analysis of variance results are shown in Tables 6 and 7. The results indicated that both models were highly significant ($p<0.0001$), and the lack-of-fit terms were not significant ($p>0.05$), indicating that the model was less affected by noise and that the regression equation fit well. The R^2 of the two models were 0.97 and 0.98, and the Predicted R^2 was in good agreement with the Adjusted R^2, indicating a strong agreement between the model and the experimental results.

Analysis of the vibration frequency results showed that *D*, *H*, D^2, and H^2 had significant effects on the vibration frequency ($p<0.001$). From the results of the analysis of vibration force, *D*, *H*, and D^2 all had a significant effect on the vibration force ($p<0.001$), with the trunk diameter having the greatest effect, followed by the trunk height effect. The model coefficients of the vibration frequency and force expressed using the coding factors are expressed in Equation (12).

$$\begin{cases} f = 17.32 + 3.12D - 0.76H - 0.07A - 0.01B - 0.09DH - \\ \quad 0.03DA + 0.09DB + 0.01HA - 0.05HB - 0.08AB + 0.75D^2 + \\ \quad 2.07H^2 + 0.19A^2 + 0.1B^2 \\ F = 14844.7 + 5123.5D + 1693.8H - 119.6A - 55.9B + 227.8DH - \\ \quad 8.3DA - 40DB + 36.8HA - 142.5HB + 141.3AB + 1883.4D^2 + \\ \quad 8.3DA - 40DB161.7H^2 - 89.5A^2 - 116.5B^2 \end{cases} \quad (12)$$

Table 5 Experimental design and results

Order	Factors				Response	
	D	H	A	B	*f* / Hz	*F* / N
1	–1	0	0	–1	17.43	13 558
2	1	0	–1	0	21.75	21 965
3	0	1	1	0	18.56	16 215
4	0	–1	0	1	20.75	13 390
5	1	0	1	0	21.56	21 470
6	0	0	1	–1	17.32	14 643
7	0	–1	1	0	20.7	13 469
8	0	1	0	1	18.41	15 862
9	1	–1	0	0	22.94	19 534
10	0	0	–1	1	17.58	14 650
11	–1	0	1	0	15.08	11 047
12	0	1	0	–1	18.58	16 393
13	0	–1	–1	0	20.81	13 676
14	0	0	–1	–1	17.33	15 031
15	–1	0	0	1	14.91	11 587
16	0	0	1	1	17.25	14 827
17	–1	–1	0	0	17.07	9810
18	0	1	–1	0	18.64	16 275
19	1	0	0	1	21.54	21 629
20	–1	0	–1	0	15.16	11 509
21	1	1	0	0	22.57	24 723
22	0	–1	0	–1	20.7	13 351
23	–1	1	0	0	17.04	14 088
24	0	0	0	0	17.38	15 268
25	1	0	0	–1	21.46	21 700
26	0	0	0	0	17.14	15 708
27	0	0	0	0	15.18	11 498

Table 6 Analysis of variance of vibration frequency

Source	Sum of squares	*df*	Mean square	*F* value	*p*-value
Model	149.83	14	10.7	33.82	< 0.0001
D	116.44	1	116.44	367.94	< 0.0001
H	7.01	1	7.01	22.14	0.0005
A	0.0533	1	0.0533	0.1685	0.6887
B	0.0014	1	0.0014	0.0045	0.9479
DH	0.0289	1	0.0289	0.0913	0.7677
DA	0.003	1	0.003	0.0096	0.9237
DB	0.0306	1	0.0306	0.0968	0.7611
HA	0.0002	1	0.0002	0.0007	0.9792
HB	0.0121	1	0.0121	0.0382	0.8482
AB	0.0256	1	0.0256	0.0809	0.7809
D^2	3.03	1	3.03	9.57	0.0093
H^2	22.8	1	22.8	72.04	< 0.0001
A^2	0.19	1	0.19	0.6004	0.4534
B^2	0.0507	1	0.0507	0.1602	0.696
Residual	3.8	12	0.3165		
Lack of fit	3.75	10	0.3749	15.6	0.0617
Pure error	0.0481	2	0.024		
Cor total	153.63	26			

Model fit statistics			
Std. dev.	0.56	R^2	0.97
Mean	18.70	Adjusted R^2	0.94
CV/%	3.01	Predicted R^2	0.85

The effect of the test factors on the response variables was analyzed using the response surface method. Figure 19 shows the contour and response plots of the effect of the trunk diameter and height on the vibration frequency and vibration force, with the other

Table 7 Analysis of variance of the vibration force

Source	Sum of squares	*df*	Mean square	*F* value	*p*-value
Model	3.74E+08	14	2.67E+07	55.18	< 0.0001
D	3.15E+08	1	3.15E+08	650.19	< 0.0001
H	3.44E+07	1	3.44E+07	71.06	< 0.0001
A	1.72E+05	1	1.72E+05	0.3542	0.5628
B	37 520.08	1	37 520.08	0.0774	0.7855
DH	2.08E+05	1	2.08E+05	0.4283	0.5252
DA	272.25	1	272.25	0.0006	0.9815
DB	6400	1	6400	0.0132	0.9104
HA	5402.25	1	5402.25	0.0112	0.9176
HB	81 225	1	81 225	0.1677	0.6894
AB	79 806.25	1	79 806.25	0.1647	0.692
D^2	1.89E+07	1	1.89E+07	39.05	< 0.0001
H^2	1.39E+05	1	1.39E+05	0.2877	0.6015
A^2	42 681.56	1	42 681.56	0.0881	0.7717
B^2	72 333.56	1	72 333.56	0.1493	0.706
Residual	5.81E+06	12	4.85E+05		
Lack of fit	3.23E+06	10	3.23E+05	0.2507	0.9468
Pure error	2.58E+06	2	1.29E+06		
Cor total	3.80E+08	26			

Model fit statistics			
Std. dev.	696.05	R^2	0.98
Mean	15 662.07	Adjusted R^2	0.97
CV/%	4.44	Predicted R^2	0.94

parameters averaged. As shown in Figure 19a and Figure 19b, the vibration frequency reached a maximum value (24.02 Hz) at the largest trunk diameter and smallest trunk height and a minimum value (13.69 Hz) at the smallest trunk diameter and smallest trunk height of 357.56 mm. The frequency of the vibration increased with an increase in the diameter of the trunk. Further, it decreased, and then increased, with an increase in the height of the trunk. As shown in Figure 19c and Figure 19d, the vibration force reached a maximum value (23935 N) at the maximum trunk diameter and height and reached a minimum value (10300 N) at the minimum trunk diameter and minimum trunk height. The vibration force increased with an increase in the trunk diameter and with an increase in the main branch height.

When the tree shape is "three open-center", the trunk diameter *D* and trunk height *H* have a significant effect on the vibration harvesting parameters. To ensure a low vibration parameter with less fruit tree damage, the main branch angle was set to 0, and the minimum value was solved using the Simple Additive Weighting method[53]. Equation (12) was scaled, and the weights of both the vibration frequency and vibration force were set to 1 and summed to obtain the objective function g (*D, H*), as shown in Equation (13) and Figure 20. As the trunk diameter *D* is usually determined by the age of the tree, it is not possible to control its exact value. The objective function value was minimal when the trunk height *H* was 600 mm. As shown in Figure 19, the objective function decreases

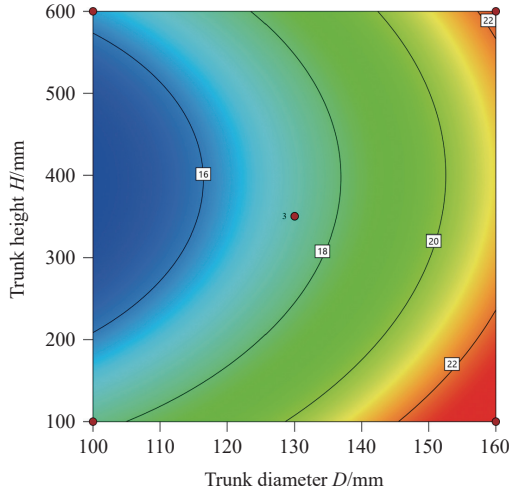

a

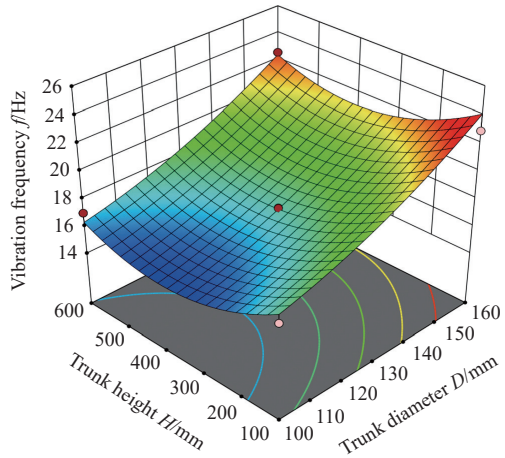

b

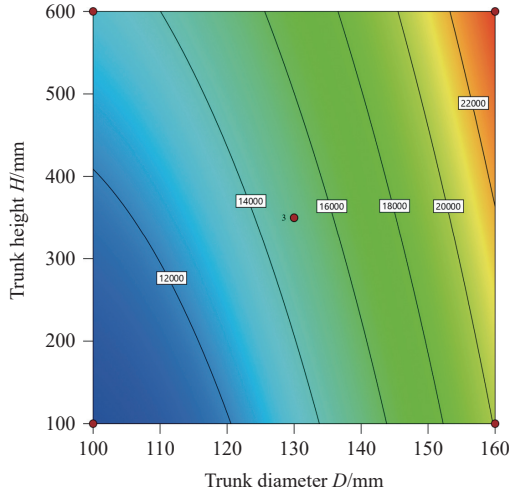

c

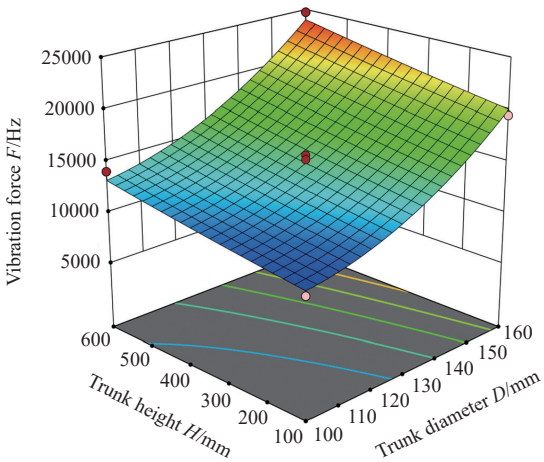

d

Figure 19 Contour and response plots of the effect of trunk diameter and height on the response variable: (a) and (b) vibration frequency; (c) and (d) vibration force, respectively

for both smaller and larger trunk heights H. Therefore, the trunk height can be set at a higher or lower level when shaping, ensuring that the parameters are consistent for all fruit trees in the orchard.

$$g(D,H) = 1.32 - 0.68D - 0.046H - 0.0083DH - 0.21D^2 - 0.21H^2 \quad (13)$$

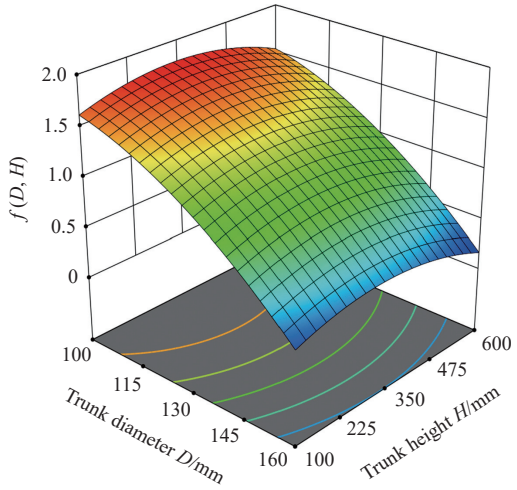

Figure 20 Objective function graph

3.5 Harvest percentage and vibration response

The morphological parameters of the olive tree were substituted into the response surface test results [Equation (9)] to obtain the vibration frequency and vibration force; the vibration time was 21 s. The harvest percentages of the three main branches were counted separately, and as listed in Table 8, the average harvest percentage of the olive fruits was 91.22%.

Table 8 Statistical analysis of experimental data on olive harvest efficiency

	Tree 1	Tree 2	Tree 3
Trunk diameter D/mm	145	153	146
Trunk height H/mm	302	118	152
Branch angle A/(°)	120	130	106
Branch angle B/(°)	125	135	136
Vibration frequency (f)/Hz	19.3	22.7	21.2
Vibration force (F)/N	17 609	18 308	16 823
Mass of vibration harvest/kg	38.456	35.829	29.953
Mass of manual harvest/kg	3.850	3.219	2.957
Harvest percentage/%	90.90	91.76	91.01

The vibration response of the fruit trees was monitored after harvesting, as shown in Figure 21. The ratio of maximum to minimum acceleration per unit of excitation was 2.2, 3.0, 3.1, and 5.4 at the four monitoring points, indicating that the vibration response varied between the monitoring locations at different vibration frequencies, with the peak acceleration per unit of excitation being the cause of the resonant response. Points 2, 3, and 4 resonate at 15 and 22.5 Hz; points 2 and 4 also resonate at 10 Hz; point 1 on the main branch has no significant resonant frequencies in the measured frequency range. According to the results of the modal analysis described in Section 3.2, the resonant frequencies of the main branch are in the lower frequency range, which is smaller than the frequency range selected for the experiment. The resonant frequency of 22.5 Hz for the three points located on the side branches is similar to the best vibration frequency of 22.7 Hz obtained from the response surface calculations in the previous section, indicating that the response surface calculations are more accurate.

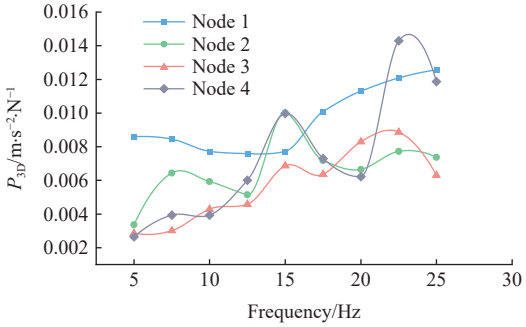

Figure 21 Dynamic response of monitoring position of olive tree under vibration excitation

4 Conclusions

Based on the vibration mode of a single eccentric block, this study proposes a method to obtain the vibration frequency and vibration force through simulation, analyze the effect of morphological parameters of the olive tree on the vibration frequency and vibration force, and verify the results through experiments. The main conclusions of this study are as follows:

1) The centrifugal force generated by the high-speed rotation of a single eccentric block can be decomposed into components of equal magnitude with a 90° difference in phase, located in the X and Y directions. The abscission acceleration of olive fruit can be simplified as the ratio of the binding force between the fruit and the stalk to the mass of the fruit, and the 90% quantile of the abscission acceleration of olive fruit was measured experimentally as 1113.35 m/s^2.

2) The vibration response of the olive tree was analyzed using simulations and experiments. The acceleration of each monitoring point of the olive tree was obtained through the rigid-flexible coupling model of the olive tree-vibration motor. The experiment was conducted using the vibration motor, and the acceleration response of the monitoring point was measured using the acceleration sensor. The results show that there is a strong correlation between the acceleration of the simulation and that of the experiment (the average correlation coefficient was 0.73) and that the rigid-flexible simulation is a good representation of the experimental results.

3) A four-factor, three-level response surface simulation experiment was designed using the main morphological parameters of the olive tree as the test factors and the vibration parameters as the response variables. The range of vibration frequencies was obtained using modal analysis. The optimum vibration frequency was obtained by sweep analysis in a rigid-flexible coupling simulation, and the optimum vibration force was obtained by monitoring the acceleration of the fruit stalk nodes under different vibration forces. A polynomial response surface model was constructed based on the response surface test, and the results showed that the trunk diameter and trunk height had significant effects on the vibration frequency and vibration force.

4) Harvesting tests were conducted on olive trees using a harvesting prototype, and the results showed that the average percentage of olive fruit harvested was approximately 91.22%. The accelerations at the four monitoring points on the main and side branches were monitored, and the results indicated that the resonance frequencies of the three points located on the side

branches were similar to those of the response surface results.

In this study, acceleration was used as a criterion for fruit abscission, and the vibration response of the olive trees was investigated through simulations and experiments. Ninety percent of olive fruit harvest was used as a target in this study to avoid damage to the harvested fruit. In future research, fruit loosening spray could be used to achieve more efficient and non-damaging mechanical harvesting.

Acknowledgements

This research was supported by the Key Research and Development Plan of Shaanxi Province (Grant No. 2024NC-ZDCYL-05-03), the Key Programs of the Joint Fund of the National Natural Science Foundation of China (Grant No. U2243235), and the Introduction of High-level Talents in Hohhot (Grant No. 2023RC-High Level-7).

[References]

[1] Romero C, Garcia A, Medina E, Ruiz-Mendez M V, de Castro A, Brenes M. Triterpenic acids in table olives. Food Chemistry, 2010; 118(3): 670–674.

[2] Wang C, Chen Q, Luo J, Bai X, Wang Y, Kong L. Development and Industrial Prospect of China's Olive. Biomass Chemical Engineering, 2013; 47(2): 41–46.

[3] FAOSTAT, 2023. Available: http://www.fao.org/faostat. Accessed on [2024-01-05].

[4] Bentaher H, Haddar M, Fakhfakh T, Maalej A. Finite elements modeling of olive tree mechanical harvesting using different shakers. Trees, 2013; 27(6): 1537–1545.

[5] Zhang Z, Lu Y. Development, evaluation and improvement of apple infield grading and sorting systems. In: Zhang Z, Zhang Z, Igathinathane C, Wang Y, Ampatzidis Y, Liu G. (Eds) Mechanical Harvest of Fresh Market Apples. Smart Agriculture, Springer, Singapore, 2022; 1: 71–87.

[6] Lu Y, Zhang Z, Lu R. Development and preliminary evaluation of a new apple harvest assist and in-field sorting machine. Applied Engineering in Agriculture, 2022; 38(1): 23–35.

[7] Liu X L, Zhang Z, Igathinathane C, Flores P, Zhang M, Li H, et al. Infield corn kernel detection using image processing, machine learning, and deep learning methodologies under natural lighting. Expert Systems with Applications, 2024; 238(E): 122278.

[8] Yu J F, Zhang Z, Mhamed M, Yuan D D, Wang X F. Apple's in-field grading and sorting technology: A review. Towards Unmanned Apple Orchard Production Cycle, 2023; 6: 81–104.

[9] Yi T J, Mhamed M. Developments in automated harvesting equipment for the apple in the orchard: Review. Smart Agricultural Technology, 2024; 9: 100491.

[10] Zhang Z, Pothula A K. Improvements and evaluation of an in-field bin filler for apple bruising and distribution. Transactions of the ASABE, 2019; 62(2): 271–280.

[11] Rui Z, Zhang Z, Chen T. A review of field plant phenotyping platform, sensing and navigation technology. Transforming Technologies in Smart Agriculture, 2024; 8: 1–46.

[12] Rui Z, Zhang Z, Zhang M, Azizi A, Igathinathane C, Cen H, et al. High-throughput proximal ground crop phenotyping systems – A comprehensive review. Computers and Electronics in Agriculture, 2024; 224: 109108.

[13] Hoshyarmanesh H, Dastgerdi H R, Ghodsi M, Khandan R, Zareinia K. Numerical and experimental vibration analysis of olive tree for optimal Optimal mechanized harvesting efficiency and productivity. Computers and Electronics in Agriculture, 2017; 132: 34–48.

[14] Zhang Z, Igathinathane C, Li J, Cen H, Lu Y, Flores P. Technology progress in mechanical harvest of fresh market apples. Computers and Electronics in Agriculture, 2020; 175: 105606.

[15] Mahamed M, Zhang Z, Yu J F, Li Y F, Zhang M. Advances in apple's automated orchard equipment: A comprehensive research. Computers and Electronics in Agriculture, 2024; 221: 108926.

[16] Yu J F, Zhang Z, Liu X H, Chen K F, Li Y X, Igathinathane C, et al. Automatic maize seeding machine watering spray angle determination by using a novel index. Computers and Electronics in Agriculture, 2024; 224: 109234.

[17] Alzoheiry A, Ghonimy M, Abd El Rahman E, Abdelwahab O, Hassan A. Improving olive mechanical harvesting using appropriate natural frequency. Journal of Agricultural Engineering, 2020; 51(3): 148–154.

[18] Castro-Garcia S, Castillo-Ruiz F J, Jimenez-Jimenez F, Gil-Ribes J A, Blanco-Roldan G L. Suitability of Spanish 'Manzanilla' table olive orchards for trunk shaker harvesting. Biosystems Engineering, 2015; 129: 388–395.

[19] Sola-Guirado R R, Bernardi B, Castro-Garcia S, Blanco-Roldan G L, Benalia S, Fazari A, Brescia A, Zhnbalatti G. Assessment of aerial and underground vibration transmission in mechanically trunk shaken olive trees. Journal of Agricultural Engineering, 2018; 49(3): 191–197.

[20] Sola-Guirado R R, Castro-Garcia S, Blanco-Roldan G L, Jimenez-Jimenez F, Castillo-Ruiz F J, Gil-Ribes J A. Traditional olive tree response to oil olive harvesting technologies. Biosystems Engineering, 2014; 118: 186–193.

[21] Aragon-Rodriguez F, Dias A B, Pinheiro A, Peça J, Días I L, Castro-Garcia S. Assessment of a side-row continuous canopy shaking harvester and its adaptability to the portuguese cobrançosa variety in high-density olive orchards. Sensors, 2023; 23(3): 1740.

[22] Castillo-Ruiz F J, Sola-Guirado R R, Castro-Garcia S, Gonzalez-Sanchez E J, Colmenero-Martinez J T, Blanco-Roldan G L. Pruning systems to adapt traditional olive orchards to new integral harvesters. Scientia Horticulturae, 2017; 220: 122–129.

[23] Castro-Garcia S, Aragon-Rodriguez F, Sola-Guirado R R, Serrano A J, Soria-Olivas E, Gil-Ribes J A. Vibration monitoring of the mechanical harvesting of citrus to improve fruit detachment efficiency. Sensors, 2019; 19(8): 1760.

[24] Yang H, San Y, Chen Y, Wang X, Niu C, Hou S. Influence of different vibration characteristic parameters on vibration response of apricot trees. Transactions of the CSAE, 2019; 35(2): 10–16.

[25] Aragon-Rodriguez F, Castro-Garcia S, Sola-Guirado R R, Gil-Ribes J A. Fruit abscission pattern of 'Valencia' orange with canopy shaker system. Scientia Horticulturae, 2019; 246: 916–920.

[26] Liu T H, Ehsani R, Toudeshki A, Abbas M, Zou X J. Shaking functionality evaluation of four different types of citrus canopy-shaker tines. Applied Engineering in Agriculture, 2018; 34(5): 809–817.

[27] Ortiz C, Torregrosa A, Castro-Garcia S. Comparison of a lightweight experimental shaker and an orchard tractor mounted trunk shaker for fresh market citrus harvesting. Agriculture, 2021; 11(11): 1092.

[28] Leone A, Romaniello R, Tamborrino A, Catalano P, Peri G. Identification of vibration frequency, acceleration, and duration for efficient olive harvesting using a trunk shaker. Transactions of the ASABE, 2015; 58(1): 19–26.

[29] Fu L, Peng J, Nan Q, He D, Yang Y, Cui Y. Simulation of vibration harvesting mechanism for sea buckthorn. Engineering in Agriculture, Environment and Food, 2016; 9(1): 101–108.

[30] Du X, Chen K, Ma Z, Wu C, Zhang G. Design, construction, and evaluation of a three-dimensional vibratory harvester for tree fruit. Applied Engineering in Agriculture, 2020; 36(2): 221–231.

[31] Wei J, Yang G Y, Yan H, Jing B B, Yu Y. Rigid-flexible coupling simulation and experimental vibration analysis of pistachio tree for optimal mechanized harvesting efficiency. Mechanics of Advanced Materials and Structures, 2021; 28(22): 2360–2369.

[32] Du X, Shen T, Chen K, Zhang G, Yao X, Chen J, Cao Y. Simulation study and field experiments on the optimal canopy shaking action for harvesting Camellia oleifera fruits. Journal of Agricultural Engineering, 2022; 53(3): 1245.

[33] Chen Q, Zhang S, Hu G, Zhou J, Zhao J, Chen Y, et al. Parameter optimization of the harvest method in the standardized hedge cultivation mode of Lycium barbarum using response surface methodology. Horticulturae, 2022; 8(4): 308.

[34] Tombesi S, Poni S, Palliotti A, Farinelli D. Mechanical vibration transmission and harvesting effectiveness is affected by the presence of branch suckers in olive trees. Biosystems Engineering, 2017; 158: 1–9.

[35] Castro-Garcia S, Aragon-Rodriguez F, Arias-Calderon R, Sola-Guirado R R, Gil-Ribes J A. The contribution of fruit and leaves to the dynamic response of secondary branches of orange trees. Biosystems Engineering, 2020; 193: 149–156.

[36] Xing H, Ma S, Liu M, Wang M, Wei Y, Hu J, et al. Evaluation of shake-and-catch methods on harvesting of tall spindle apples. Transactions of the ASABE, 2020; 63(4): 857–863.

[37] Afsah-Hejri L, Homayouni T, Toudeshki A, Ehsani R, Ferguson L, Castro-García S. Mechanical harvesting of selected temperate and tropical fruit and nut trees. Horticultural Reviews, 2021; 49: 171–242.

[38] Xu N, Du X, Liu E, Li D, Du J, Wu C. Analysis of the hickory tree motion under the excitation of eccentric-type vibratory mechanism. In: 2017 ASABE Annual International Meeting, 2017; doi: 10.13031/aim.201700772.

[39] Chen D, Du X, Wang S, Zhang Q. Mechanism of vibratory fruit harvest and review of current advance. Transactions of the CSAE, 2011; 27(8): 195–200.

[40] San Y, Yang H, Wang X, Guo W, Hou S. Dynamic response analysis of apricot fruit dropping during vibration harvesting. Transactions of the CSAE, 2018; 34(18): 68–75.

[41] Wu D, Zhao E, Jiang S, Ding D, Liu Y, Liu L. Optimization analysis and test of canopy vibration parameters of camellia fruit based on double pendulum model. Transactions of the CSAM, 2021; 52(12): 96–104.

[42] Araújo e Silva Ferraz G, da Silva F M, de Carvalho Alves M, de Lima Bueno R, da Costa P A N. Geostatistical analysis of fruit yield and detachment force in coffee. Precision Agriculture, 2012; 13(1): 76–89.

[43] Niu Z J, Xu Z, Deng J T, Zhang J, Pan S J, Mu H T. Optimal vibration parameters for olive harvesting from finite element analysis and vibration tests. Biosystems Engineering, 2022; 215: 228–238.

[44] Peng J, Xie H Q, Feng Y L, Fu L S, Sun S P, Cui Y J. Simulation study of vibratory harvesting of Chinese winter jujube (*Zizyphus jujuba* Mill cv. Dongzao). Computers and Electronics in Agriculture, 2017; 143: 57–65.

[45] Chen Y, Zhao J, Hu G R, Chen J. Design and testing of a pneumatic oscillating Chinese wolfberry harvester. Horticulturae, 2021; 7(8): 214.

[46] Vu V D, Ngo Q H, Nguyen T T, Nguyen H C, Nguyen Q T, Nguyen V D. Multi-objective optimisation of cutting force and cutting power in chopping agricultural residues. Biosystems Engineering, 2020; 191: 107–115.

[47] Sola-Guirado R R, Aragon-Rodriguez F, Castro-Garcia S, Gil-Ribes J. The vibration behaviour of hedgerow olive trees in response to mechanical harvesting with straddle harvester. Biosystems Engineering, 2019; 184: 81–89.

[48] Tang X, Ren J, Liu C, Xiao D. Simulation of vibration harvesting mechanism for wolfberry. In: ASABE Annual International Meeting, 2011. doi: 10.13031/2013.37391.

[49] Mucchielli P, Bhowmik B, Hazra B, Pakrashi V. Higher-order stabilized perturbation for recursive eigen-decomposition estimation. Journal of Vibration and Acoustics-Transactions of the ASME, 2020; 142(6). doi: 10.1115/1.4047302

[50] Savary S K J U, Ehsani R, Schueller J K, Rajaraman B P. Simulation study of citrus tree canopy motion during harvesting using a canopy shaker. Transactions of the ASABE, 2010; 53(5): 1373–1381.

[51] Carvalho E d A, Magalhães R R, Santos F L. Geometric modeling of a coffee plant for displacements prediction. Computers and Electronics in Agriculture, 2016; 123: 57–63.

[52] Villibor G P, Santos F L, de Queiroz D M, Junior J K K, de Assis de Carvalho Pinto F. Dynamic behavior of coffee fruit-stem system using modeling of flexible bodies. Computers and Electronics in Agriculture, 2019; 166: 105009.

[53] Wang Y J. A fuzzy multi-criteria decision-making model based on simple additive weighting method and relative preference relation. Applied Soft Computing, 2015; 30: 412–420.